F. Arzour[1], M. Hadj Meliani[1], A. Jabbar Hassan[2], T. Boukharouba[2]

MICROSTRUCTURE EVOLUTION IN FRICTION WELDING OF AISI 316

EVOLUCIJA MIKROSTRUKTURE ČELIKA AISI 316 TOKOM ZAVARIVANJA TRENJEM

Originalni naučni rad / Original scientific paper
UDK /UDC:

Rad primljen / Paper received: 23.12.2019

Adresa autora / Author's address:
[1)] LPTPM, Hassiba Ben Bouali University of Chlef, Chlef, Algeria, email: m.hadjmeliani@univ-chlef.dz
[2)] Laboratoire de Mécanique Avancée 'LMA', University of Science and Tech. of Houari Boumediene, Algiers, Algeria

Keywords
- austenitic stainless steel
- heat flow
- microstructure
- welding stages

Ključne reči
- austenitni nerđajući čelik
- prostiranje toplote
- mikrostruktura
- faze zavarivanja

Abstract

The evolution of mechanical properties of steel AISI 316 during direct drive friction welding depends essentially on the heat flow. The generation of this flow depends on two parameters, rotation speed and friction pressure. In the first instance, the optimisation of welding conditions is made to obtain a microstructure closest to that of the base metal. This optimisation is made for a single parameter; the temperature must remain below the phase transformation line, 926 °C for AISI 316 /1, 2/. Results show that the microstructure of the welded joint is built in the last three steps of the process. During the first step of friction phase, the application of friction pressure causes cold deformation creating a mechanical deformation zone (MDZ_1). At the second step of friction phase, MDZ_1 leaves place for softening zone, because of heat diffusion, with a remaining friction pressure. The thermomechanically affected zone (TMAZ) is the final step of the friction phase. The forging pressure applied in the third step defines the microstructure of the welded joint; the TMAZ is replaced by the second mechanical deformation zone (MDZ_2). Additionally, forging pressure application creates inside the new MDZ_2 a hard eccentric core around the weld centre, precisely along the rotation axis. The microhardness of MDZ_2 is higher than TMAZ and less than MDZ_1. Post welding analyses were investigated by microhardness measurements, SEM, and tensile tests. They illustrate the important role of heat flux on the joint microstructure through the welding process.

Izvod

Evolucija mehaničkih osobina čelika AISI 316 tokom zavarivanja direktnim trenjem u suštini zavisi od prostiranja toplote. Generisanje ovog toka zavisi od dva parametra – brzine rotacije i pritiska od trenja. Ovde je po prvi put prikazana optimizacija parametara i uslova zavarivanja kako bi se dobile mikrostrukture približne osnovnom materijalu. Ova optimizacija je urađena za jedan parametar; temperatura treba da je ispod linije fazne transformacije, 926 °C za AISI 316 /1, 2/. Rezultati su pokazali se mikrostruktura zavarenog spoja formira u poslednja tri koraka postupka zavarivanja. U prvom koraku faze trenja, pritisak od trenja prouzrokuje hladnu deformaciju i stvara prvu zonu plastične deformacije (MDZ_1). U drugom koraku faze trenja, MZD_1 omekšava usled difuzije toplote, pod dejstvom pritiska. Zona termomehaničkog uticaja (TMAZ) nastaje tokom poslednjeg koraka faze trenja. Pritisak kovanja koji deluje tokom trećeg koraka definiše mikrostrukturu zavarenog spoja; TMAZ prelazi u drugu zonu plastične deformacije (MDZ_2). Osim toga, unutar MDZ_2 pritisak kovanja stvara tvrdo ekscentrično jezgro oko centra šava, duž ose rotacije. Mikrotvrdoća MDZ_2 je veća od TMAZ, a manja od MDZ_1. Analize posle zavarivanja su obuhvatile merenje mikrotvrdoće, skening elektronska mikroskopija i ispitivanja zatezanjem. Ova ispitivanja potvrđuju značajan uticaj toplotnog fluksa na mikrostrukturu zavarenog spoja tokom postupka zavarivanja.

INTRODUCTION

The advantage of solid state welding is the elimination of the hot cracking problem, /3/. A filler metal is not necessary, which avoids the formation of hard and brittle phases. The welded joint remains chemically homogeneous; another advantage constitutes low effect of corrosion, /3/. The equipment is simple, needs little maintenance and experience. Overall, the process is clean, no smoke, no danger, fast and automated that guarantees control of its parameters /4-6/. In the present work, for example, the longest welding operation does not exceed 20 s. This joining process is associated with both mechanical and thermal effects. The mechanical effect is primarily related to friction pressure while the thermal effect depends on the friction time. The mechanical effect occurs before the elevation of temperature, during the friction contact phase. This effect ends at maximal temperature and the thermal effect begins. This last is stopped also at the end of the friction phase. The mechanical effect appears again with forging pressure application. The history of microstructural evolution passes through four stages, that form the three phases of direct drive friction welding (frictional contact phase, friction and forge phase). Future mechanical properties of welded joint depend on this history of the base metal. This method allows separating both mechanical and thermal effects during the welding operation in order to evaluate the effect and role of each

step in the microstructural evolution of the welded joint. So, to conclude that as the following:

– first step of friction phase leads to finer grain size with increase of hardness,
– grain growth with decrease of hardness occurs in the second step of the friction phase,
– the unique step of the forging phase introduces a second mechanical effect by creating a hard core, benefiting from the remaining thermal effect (second step of the friction phase).

EXPERIMENTAL STUDY

The material used is austenitic stainless steel AISI 316, with chemical composition, mechanical and physical properties of the base metal shown respectively in Tables 1, 2 and 3.

Table 1. Chemical composition of base metal (wt. %).

C	Mn	Si	P	S	Mo	Cr	Ni
0.04	1.50	0.67	0.03	0.021	2.93	17.93	9.95

Table 2. Mechanical properties of base metal.

Offset Yield Stress 0.01 % (MPa)	UTS (MPa)	Modulus of elasticity (MPa)	Elongation (%)	Average micro-hardness ($HV_{0.1}$)	Strain hardening exponent, n	Strength coefficient K (MPa)
578	670 – 680	$\approx 1.93 \cdot 10^5$	≈ 45	260 – 263	0.206	1146

Table 3. Physical properties of base metal, /7/.

Steel grade	Yield stress σ_y (MPa)	Ultimate strength σ_u (MPa)	Elongation (%)	Reduction of area (%)	Fracture toughness K_{Ic} (MPa$\sqrt{m}$)	Hardness HV
API X65	465	558	11	57	280	205
API X52	410	528	23	--	116.6	--

Table 4. Average value results of friction welding of selected cases.

Case	RS (min^{-1})	AT (s)	FrP (MPa)	FrT (s)	FoP (MPa)	FoT (s)	UD (mm)	T_{max} (°C)	AITss (E0-E1) (°C/s)
X4	3000	3.5	4.50	8.50	8.00	5.00	11.75	870	0.0013789
X2			3.50	8.50	8.00		8.00	790	0.0015187
X5			4.00	6.50	8.00		8.75	819	0.0014703

RS-rotation speed; AT-friction contact time; FrP-friction pressure; FrT-friction time; FoP-forging pressure; FoT-forging time; UD-upset distance; T_{max}-maximum temperature; AITss-average increasing temperature, solid state

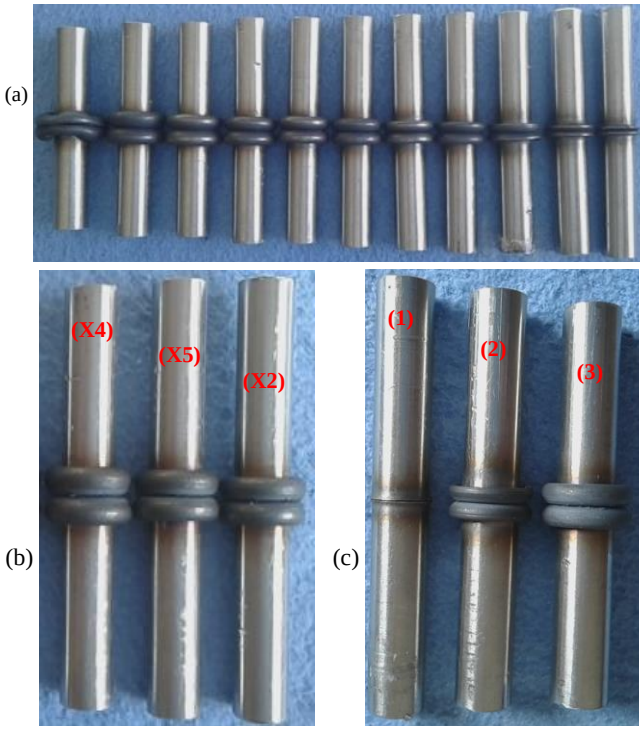

Figure 1. AISI 316 specimens with welding conditions: a) different flash metal according to parameters; b) X4, X5 and X2; c) steps of X5 (1) E0-E1, (2) E1-E2 and (3) E2-E3.

This study begins by optimising the welding parameters which are controlling the flow of heat generated during the process. The temperature is measured at two positions by using two thermocouples. The first is a thermocouple type K (attached by cold welding), and second one is an infrared thermocouple. The average uncertainty of measurement is 45 °C, observed for 107 operations with 11 conditions have been fulfilled (Fig. 1a). That seems in both cases X4 and X5 (Table 4), while the friction pressure and rotation speed used for both cases are the same. The welding operations are achieved without any preparation of cutting samples. Before the welding process specimens are cut directly from 6 m bars at 45 mm length and 12 mm diameter, followed by a face machining for the welding interface preparation.

The selected conditions were used in the present study (Fig. 1b) subjected to limiting temperature of 926 °C, which must remain below the phase transformation, /8/. For example, two of the cases:

1. Rejected case (X1, does not exist in Table 4), maximal temperature 1057 °C > phase transformation temperature with upset distance 16 mm.
2. Retained case (X5, Table 4), maximal temperature 819 °C < phase transformation temperature, with 8.75 mm upset distance (Fig. 1c).

The study shows macro- and microscopic levels for three cases: X2, X4 and X5 (Figs. 1b and Table 4). Each case represents the mean value of seven or six welding operations. The history of microstructural evolution is subjected to four steps, contained in three phases that define the welding operation (Table 5). Three of them are illustrated in Fig. 1c. The temperature level generated in the welding operation depends on friction pressure, speed of rotation and the physical properties of the material. The welding operation starts with the frictional contact phase, at the instant of applied frictional pressure. The duration of this

phase depends on rotation speed, specific heat, friction coefficient and density of welded material. At the end of this first phase, the temperature begins to increase locally at the interface (Fig. 2), indicating the onset of the most important phase, called the friction phase, consisting of two steps. The first step of the friction phase occurs when the metal is heated locally to maximal temperature. The upset rate for AISI 316 at the end of this step can exceed 14 % (Fig. 2), and it is the start of flash metal formation (Fig. 1c). The change in temperature is roughly linear and the maximal temperature reached depends on rotation speed and friction pressure (Table 4). Once arrived at maximal temperature, the second step of the friction phase starts. The metal begins to soften, leading to friction and temperature decrease that allows for flash metal formation. The physical flash metal is produced from the soft metal which extrudes to the free circumference of the welded piece, and this first migration of grains is contained until the end of the friction time (Fig. 1c). The upset rate during this second step of friction phase can exceed 57 % of total upset rate and it depends mainly on friction time and pressure (Table 4).

The friction pressure is replaced by forging pressure at the sudden stop of rotation. Under the effect of this pressure, the metal is not yet completely cold (T > 350 °C, for case X5), so it has to be continuously discharged from centre to the circumference of the welded piece, /9/. The upset rate during this phase does not exceed 30 % of the total upset rate in the X5 case.

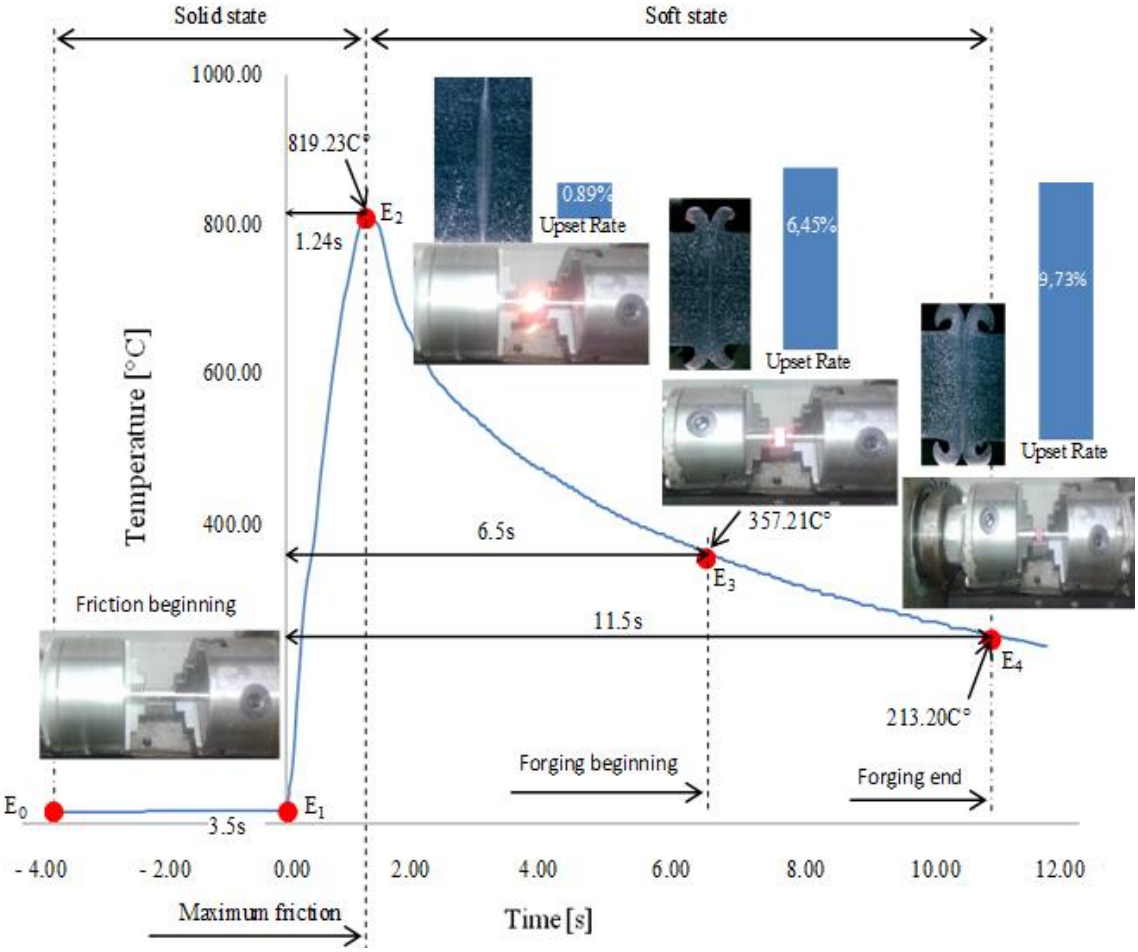

Figure 2. Temperature distribution during friction welding stages.

Table 5. Four steps (three phases) of direct drive friction welding.

Steps	Metal state	Description	Phase
1/ E_0 - E_1	solid state	Start of friction, this phase ends when the temperature at the interface of the two parts exceeds room temperature (Fig. 2).	frictional contact
2/E_1 - E_2	solid state	Future microstructure of the metal depends principally on this step. This is clearly seen in the macrograph, large mechanically affected zone along the perpendicular axis to the welding axis. The measured surface temperature reaches its maximum value at the end of this stage (Fig. 2).	friction
3/E_2 - E_3	soft state	Heat dissipation depends on friction time remaining after the first step of friction. The dissipation can exceed 55 % of the maximal value of temperature measured at the surface. The flash metal is formed at least 50 % (Fig. 2).	friction
4/E_3 - E_4	soft state	Temperature continues to fall to 75 % of its maximal value at the end of the fourth stage (Fig. 2). The flash metal takes its final form at the end of this phase (E_4).	forging

MECHANICAL TESTS

The evolution of deformation during the test is measured locally, using a displacement sensor with an open space 19.5 mm ± 2.5. The sensor is mounted on the test piece around the interface of the welded joint. An example of comparing seven tensile curves is shown in Fig. 3.

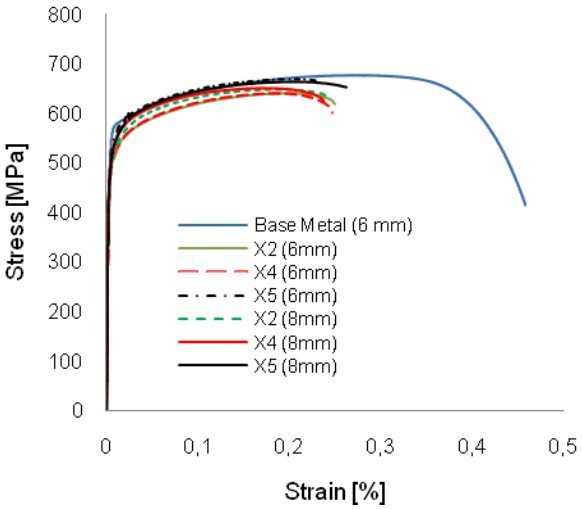

Figure 3. Tensile test curves.

Test results show that plastic deformation tends to be localized beyond the hard core, i.e. in the softest zones (TMAZ_2) away from the weld interface, /10/. For the three cases, the fracture position is in the stationary part of welded specimens (Fig. 4), which presents more ductility than the rotating part. Disregarding the accuracy of the tensile test, there are differences between results obtained from base metal and welded specimens. These differences reveal three characteristics (Table 6):

– total strain,
– ultimate tensile stress UTS,
– strain related to UTS.

Generally, according to mechanical properties obtained by tensile tests, the X5 case is the closest to mechanical properties of the base metal (Table 6).

Figure 4: Tensile test fracture

Table 6. Tensile test results.

Dia. (mm)	Case	σ_{max} (MPa)	ε at σ_{max}	ε_{max} (%)	$\frac{\sigma_{max,\ welded}}{\sigma_{max,\ base\ metal}}$ (%)	$\frac{\varepsilon_{max,\ welded}}{\varepsilon_{max,\ base\ metal}}$ (%)
6	Base metal	678.17	0.274	0.457		
	X2	641.206	0.187	0.25	5.45	45.30
	X4	641.344	0.2	0.247	5.43	45.95
	X5	670.134	0.209	0.231	1.18	49.45
8	X2	649.212	0.191	0.24	4.27	47.48
	X4	651.373	0.172	0.237	3.95	48.14
	X5	663.689	0.202	0.262	2.14	42.67

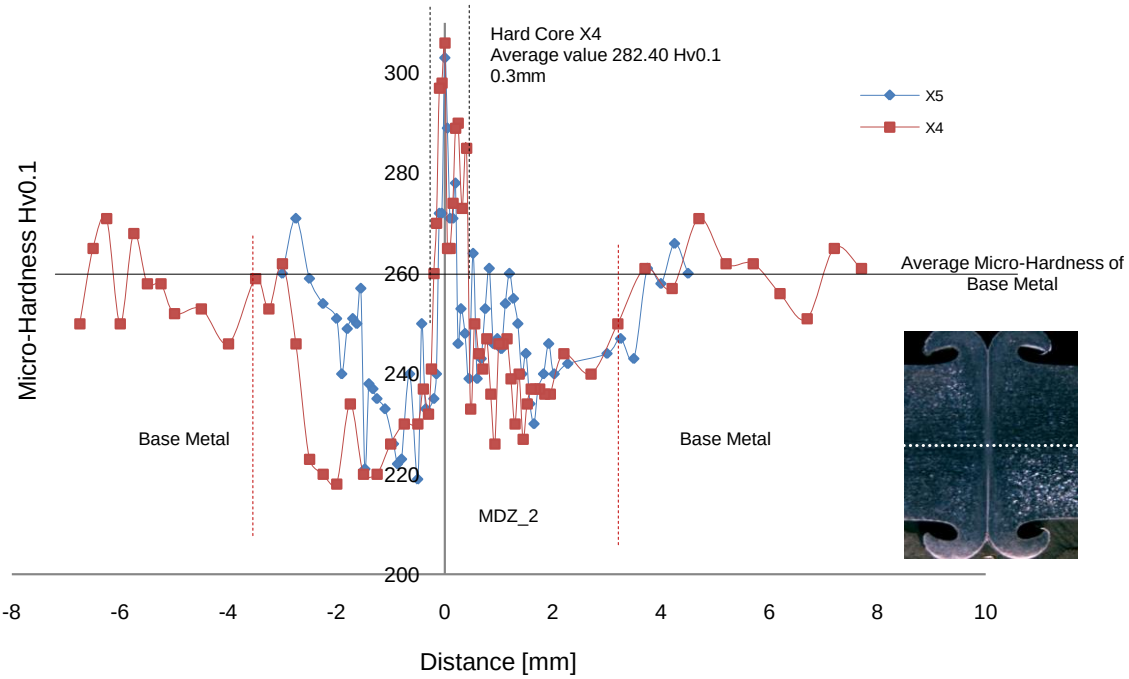

Figure 5. Comparison between cases X4 and X5.

MICROHARDNESS TEST

Microhardness measurements along the welding direction allowed estimating of local micromechanical properties around the weld interface. Microhardness profiles for cases X4 and X5 are represented by plots both side along the welding central axis (Fig. 5), the stationary part is denoted by the (–) side and the rotating part is designated by the (+) side. The specimens are mechanically polished up to 5 μm. Measurements are carried out by using 100 g indenter weight (HV0.1). A total of 7 measurements are made for the base metal at different locations with an average of 17 units of uncertainty.

CONCLUSION

The first example of friction welding was in 1860, and then while introducing manufacturing applications in the middle of the 20th century. Since then, many scientists have researched this process by using different analyses to explain the mechanism that controls the direct drive friction welding. The present study uses a simple plan and tries to explain the mechanism controlling the microstructure of the obtained welded joint. The final structure depends on the last three steps of the process. Each of the three steps provide a new microstructure. The first fine grain zone results by cold deformation under mechanical action and rotation speed. This last zone is transformed by diffusion of heat flow associated with mechanical action resulting in the grain growth zone deformed by torsion. This zone also transforms, under the effect of shear due to another cold deformation, to a zone with grain size near to that of the base metal, which covers a narrow fine grain zone that has a microhardness higher than the base metal. This fine grain zone of cylindrical form is named by a hard core.

REFERENCES

1. Nishio, Y., Ohmae, T., Yoshida, Y, Miura, Y. (1971), *Weld cracking and mechanical properties of 17% chromium steel weldment*, Weld. Res. Suppl., Weld. J. 50(1): 9s-18s.
2. Castro, R.J., Cadenet, J.J., Welding Metallurgy of Stainless and Heat-Resisting Steel, Cambridge University Press, Cambridge, 1975.
3. Genevois, C., *Genèse des microstructures lors du soudage par friction malaxage d'alliages d'aluminium de la série 2000 & 5000 et comportement mécanique résultant*, Thèse de Doctorat, Institut National Polytechnique 'INPG' de Grenoble, France, 2004, Spécialité: Science et Génie des matériaux, Ecole Doctorale Matériaux et Génie des Procédés. (in French)
4. Avinash, M., Chaitanya, G.V.K., Kumar Giri, D., et al. (2007), *Microstructure and mechanical behaviour of rotary friction welded titanium alloys*, World Acad. Science, Eng. Tech., Int. J Mater. Metall. Eng. 1(11): 641-643.
5. Faes, K., Dhooge, A., Baets, P. De, Afschrift, P. (2009), *New friction welding process for pipeline girth welds-welding time optimisation*, Int. J Adv. Manuf. Techn. 43: 982-992. doi: 10.1007/s00170-008-1775-z
6. Bonte, D., Derynck, B., De Baets, P., et al. (2010), *Friction welding of ceramics to metals*, in Day of Research Proc. 2010, Sustainable Construction & Design, Vol. 1, Ed. Jeroen Van Wittenberghe, Laboratory Soete, Ghent University, Ghent, Belgium, pp. 14-20.
7. AK Steel Corporation, 9227 Centre Pointe Drive, West Chester, OH 45069, USA. www.aksteel.com (last visited Feb. 2020).
8. Asif, M.M., Shrikrishna, K.A., Sathiya, P. (2016), *Effects of post weld heat treatment on friction welded duplex stainless steel joints*, J Manuf. Processes 21(C): 196-200. doi: 10.1016/j.jmapro.2015.10.005
9. Hazra, M., Rao, K.S., Reddy, G.M. (2014), *Friction welding of a nickel free high nitrogen steel: Influence of forge force on microstructure, mechanical properties and pitting corrosion resistance*, J Mater. Res. Technol. 3(1): 90-100. doi: 10.1016/j.jmrt.2013.12.001
10. Ajith, P.M., Barik, B.K., Sathiya, P., Aravindan, S. (2015), *Multiobjective optimization of friction welding of UNS S32205 duplex stainless steel*, Defence Technol. 11(2): 157-165. doi: 10.1016/j.dt.2015.03.001